

Charged Pion Energy Reconstruction in the ATLAS Barrel Calorimeter

M. Bosman

*Universitat Autònoma de Barcelona
Institut de Física d'Altes Energies
Barcelona, Spain*

Y. Kulchitsky

*JINR, Dubna, Russia
⊗ Institute of Physics,
National Academy of Sciences, Minsk, Belarus*

M. Nesi

CERN, Geneva, Switzerland

Abstract

The intrinsic performance of the ATLAS barrel and extended barrel calorimeters for the measurement of charged pions is presented. Pion energy scans ($E = 20, 50, 200, 400$ and 1000 GeV) at two pseudo-rapidity points ($\eta = 0.3$ and 1.3) and pseudorapidity scans ($-0.2 < \eta < 1.8$) with pions of constant transverse energy ($E_T = 20$ and 50 GeV) are analysed. A simple approach, that accounts in first order for non-compensation and dead material effects, is used for the pion energy reconstruction. The intrinsic performances of the calorimeter are studied: resolution, linearity, effect of dead material, tails in the energy distribution. The effect of electronic noise, cell energy cuts and restricted cone size are investigated.

1 ATLAS Calorimetry

A view of the ATLAS calorimeters [1] is presented in Figure 1. The calorimetry consists of an electromagnetic (EM) calorimeter covering the pseudorapidity region $|\eta| < 3.2$, a hadronic barrel calorimeter covering $|\eta| < 1.7$, hadronic end-cap calorimeters covering $1.5 < |\eta| < 3.2$, and forward calorimeters covering $3.1 < |\eta| < 4.9$.

The EM calorimeter is a lead/liquid-argon (LAr) detector with accordion geometry [2]. Over the pseudorapidity range $|\eta| < 1.8$, it is preceded by a presampler detector, installed immediately behind the cryostat cold wall, and used to correct for the energy lost in the material upstream of the calorimeter.

The hadronic calorimetry of ATLAS, presented in Figure 1, consists of three main devices. In the barrel region ($|\eta| < 1.7$) there is the scintillating Tile Calorimeter [3]. The Hadronic End-cap LAr Calorimeter (HEC) extends up to $|\eta| = 3.2$. The range $3.1 < |\eta| < 4.9$ is covered by the high density Forward Calorimeter (FCAL). Up to $|\eta| = 2.5$ the basic granularity of the hadron calorimeters is $\Delta\eta \times \Delta\phi = 0.1 \times 0.1$. This region is used for precise measurements of the energy and angles of jets. In the region $|\eta| > 2.5$, the basic granularity is approximately $\Delta\eta \times \Delta\phi = 0.2 \times 0.2$.

A more detailed description of all ATLAS calorimeters is given in the Calorimeter TDRs ([1], [2] and [3]).

The performance of the barrel and extended barrel sections of the ATLAS hadronic calorimeter for the measurement of charged pion energy is studied. The intrinsic energy resolution, the effects of dead material, electronic noise and limited cone size are discussed.

2 Energy Resolution

In the barrel region, the response of the calorimeter was studied at two pseudorapidity values: $\eta = 0.3$ (central barrel) and $\eta = 1.3$ (extended barrel). First, the energy sampled in the different calorimeter compartments is converted to the total deposited energy using the electromagnetic energy scale (EM scale). The intrinsic performance of the calorimeter is studied: the energy considered is not restricted to a cone and electronic noise is not added. These effects are discussed later in Section 4. The algorithm to reconstruct the pion energy is similar to the "Benchmark Method" used

to analyse the combined LAr-Tile test beam data [4]

$$E_{rec} = \alpha \cdot E_{had} + \beta \cdot E_{em} + \gamma E_{em}^2 + \delta \cdot \sqrt{E_{had\ 1} \cdot E_{em\ 3}} + \kappa \cdot E_{ITC} + \lambda \cdot E_{scint} . \quad (1)$$

The coefficients α and β take into account the different response of the EM and Hadronic Calorimeters to the pion energy. The quadratic term γE_{em}^2 provides an additional first order correction for non-compensation (the coefficient is negative, it suppresses the signal for events with a large fraction of electromagnetic energy). The term $\delta \sqrt{E_{had\ 1} \cdot E_{em\ 3}}$ estimates the energy loss in the cryostat wall separating the LAr and Tile Calorimeters. In the central barrel, the energy is taken from the geometric mean of the energies in the last compartment of the LAr EM barrel ($E_{em\ 3}$) and the first compartment of the Tile barrel calorimeter ($E_{had\ 1}$); whereas in the extended barrel the energy is taken from the geometric mean of the energies in the outer wheel of the EM end-cap and the first compartment of the Tile extended barrel calorimeter. The term κE_{ITC} corrects for the energy loss in the dead material in the vertical gap between the Tile central and extended barrels. It is sampled by the two Intermediate Tile Calorimeter (ITC) modules (see Figure 2). The last term λE_{scint} corrects for the energy loss in the barrel and end-cap vertical cryostat walls (see Figure 2).

The response and the energy resolution for pions in the energy range from $E_0 = 20\ GeV$ to $1\ TeV$ at $\eta = 0.3$ and 1.3 are shown in Figures 3 and 4. The open crosses show the results when the coefficients of Equation (1) are independent of energy. With the simple "Benchmark Method", the effect of non-compensation is not fully corrected for and there is a residual non-linearity of the pion response of the order of 4 – 5% between 20 GeV and 1 TeV. The test beam data show a 10% residual non-linearity between 20 and 300 GeV when using the same reconstruction method [4], reflecting the fact that G-CALOR [5] predicts a lower degree of non-compensation and may not describe correctly the energy dependence of the fraction of electromagnetic energy produced in the pion interaction. The energy dependence of the resolution is fitted with the two-term formula

$$\sigma/E = a/\sqrt{E} \oplus b \quad (2)$$

where the sampling term a is given in $\% \sqrt{GeV}$ and the constant term b in $\%$. Although the resolutions obtained for low-energy pions are similar in both cases, at high energy there is some longitudinal leakage in the central

barrel, yielding a resolution at 1 TeV of 3% instead of the 2% obtained in the extended barrel. When energy dependent parameters are applied (solid dots), the linearity of the response is restored ¹ and the resolution improved. The results are presented in Table 1:

Table 1: Terms of the pion energy resolution for the $\eta = 0.3$ and 1.3 (results of the fit with Equation (2)).

η	a (% $\sqrt{\text{GeV}}$)	b (%)
0.3	40 ± 1	3.0 ± 0.1
1.3	44 ± 3	1.6 ± 0.3

3 Pseudorapidity Scan

A pseudorapidity scan with pions of constant transverse energy $E_T = 20$ and 50 GeV was carried out to check that the linearity of the response can be maintained across the pseudorapidity range covered by the barrel and the extended barrel, and that no significant tail appears in the line shape. The algorithm, characterised by Equation (1), with energy dependent parameters was applied. The parameters were adjusted independently for the six sets of pion data, each one covering an interval of 0.4 in pseudorapidity.

The energy resolutions obtained for the two scans are shown in Figure 5. The solid lines show the energy resolution corresponding to Equation $\sigma/E = 39\%/\sqrt{E} \oplus 1\%$ for $E_T = 20$ GeV and $\sigma/E = 49\%/\sqrt{E} \oplus 2\%$ for $E_T = 50$ GeV. This performance allows to fulfil the goal for the jet energy resolution of the ATLAS hadronic calorimetry in the region $|\eta| < 3$ of $\sigma/E = 50\%/\sqrt{E} \oplus 3\%$.

In the region of the cracks between the calorimeters, from about $|\eta| = 1.3$ to $|\eta| = 1.5$, where the amount of dead material is the largest, the resolution is somewhat worse.

¹The 1% residual non-linearity at 20 GeV results from the fact that the coefficients were obtained by minimizing the expression $\sum (E_{rec} - E_0)^2$ without the addition of a linear term $\sum (E_{rec} - E_0)$ with a Lagrange multiplier.

Figure 6 shows the linearity of the response across η . The fitted mean is plotted for each interval of 0.05 in η . The RMS of the mean is 1.1% for $E_T = 50$ GeV and 2.0% for $E_T = 20$ GeV.

In addition, the tails of the distributions of the reconstructed energy were investigated. Figure 7 shows the events with a pion response more than three standard deviations away from the mean. No significant tails are present: the fraction of events in the tails does not exceed 1 – 2%. A few events out of a total of 5000 events per energy scan, mostly from the sample of pions of $E_T = 20$ GeV, deposit relatively little energy. These correspond to pions decaying to muons before reaching the calorimeter.

4 Effects of Electronic Noise and Cone Size

The results presented so far were obtained without any restriction on the pion reconstruction volume. These results characterise the intrinsic performance of the calorimeters. The presence of electronic noise does not allow integration over a too wide region, therefore the measurement of the pion energy must be restricted to a cone

$$\Delta R = \sqrt{\Delta^2\eta + \Delta^2\phi} . \quad (3)$$

A compromise has to be found between the pion energy lost outside of this cone and the noise included inside. The optimum varies as a function of pseudorapidity, since the showers have a width which is characterised by the polar angle whereas the calorimeter cells subtend intervals of constant pseudorapidity. Hence, at higher values of pseudorapidity, the showers extend laterally over more cells.

For a cone of $\Delta R = 0.6$ ($\Delta R = 0.3$), the noise is above 3 GeV (1.5 GeV). Digital filtering [6] allows noise suppression (approximately by a factor 1.6). But even this level of noise is large and is comparable to the intrinsic resolution of the calorimeters for pions with energy of a few tens of GeV. A smaller cone of $\Delta R = 0.3$ is preferable from this point of view; after digital filtering, noise can be kept around 1 GeV in the barrel region and below 3 GeV in the pseudorapidity region covered by the extended barrel.

The response and the energy resolution in the barrel region are presented in Figures 8 and 9 as a function of the cone size used for the pion energy reconstruction. Energy losses outside a cone noticeably increase

with decreasing cone size, especially for 50 GeV pions. The energy resolution also becomes worse, but it is still acceptable for the cone of $\Delta R = 0.3$.

Selecting cells with energy deposition above a certain threshold decreases the noise contribution. A study to optimise the cone size and the noise cut was performed in the barrel region. A 2σ -noise applied to the calorimeter cells within a cone of $\Delta R = 0.3$ leads to the best energy resolution. In Figure 10, the energy dependency of the resolution is plotted for two pseudorapidities: $\eta = 0.3$ and $\eta = 1.3$. The energy dependence of the resolution can be parametrised by the equation 2 with an additional noise term:

$$\sigma/E = a/\sqrt{E} \oplus b \oplus c/E \quad (4)$$

where c is given in $\%GeV$. The results of the fit with the formula of Equation 4 are presented in Table 2.

Table 2: Terms of the pion energy resolution fitted with the two-term (2) and the tree-term (4) expression for the $\eta = 0.3$ and 1.3.

Central barrel region $\eta = 0.3$			Extended barrel region $\eta = 1.3$		
a (% \sqrt{GeV})	b (%)	c (GeV)	a (% \sqrt{GeV})	b (%)	c (GeV)
No Cone, No Noise					
40 ± 1	3.0 ± 0.1	–	44 ± 3	1.6 ± 0.3	–
Cone $\Delta R = 0.3$, No Noise					
53 ± 2	3.0 ± 0.2	–	67 ± 4	2.9 ± 0.4	–
Cone $\Delta R = 0.3$, Noise with a 2σ -cut					
50 ± 4	3.4 ± 0.3	fixed at 1.0	68 ± 8	3.0 ± 0.7	fixed at 1.5

5 Conclusions

The response of the barrel and extended barrel region of the ATLAS calorimeter system to single charge pions was investigated using full simulation. Pion energy scans from $E = 20$ GeV to 1000 GeV and pseudo-rapidity scans with pions of constant transverse energy ($E_T = 20$ and

50 GeV) have been analysed. For the pion energy reconstruction, the "Benchmark approach" was used: it provides a first order correction for non-compensation effects and accounts for the effect of the dead material by using the ITC's and scintillators to sample the energy loss or interpolating between the energy deposited in adjacent calorimeter layers.

Energy and rapidity dependent and independent calibrations have been considered. The best results are obtained with energy and rapidity dependent parameters. The effect of electronic noise has been studied: cone size and cell energy cuts have been optimised. The energy dependence of the resolution can be parameterized as: $(50 \pm 4)\%/\sqrt{E} \oplus (3.4 \pm 0.3)\% \oplus 1.0/E$ at $\eta = 0.3$ and $(68 \pm 8)\%/\sqrt{E} \oplus (3.0 \pm 0.7)\% \oplus 1.5/E$ at $\eta = 1.3$. The larger constant term at $\eta = 0.3$ can be explained by the longitudinal leakage from calorimeters in this region. The resolution, obtained for the pseudorapidity scans, is represented by: $(39 \pm 1)\%/\sqrt{E} \oplus (1 \pm 5)\%$ for $E_T = 20$ GeV, $(49 \pm 9)\%/\sqrt{E} \oplus (2 \pm 6)\%$ for $E_T = 50$ GeV, in the full range, except from about $|\eta| = 1.3$ to $|\eta| = 1.5$, where the resolution is deteriorated by the energy loss in the dead material although no significant tails in the energy spectrum appears.

Acknowledgements

The authors are grateful to Andrei Kiryunin for fruitful discussions.

References

- [1] ATLAS Collaboration, Calorimeter Performance Technical Design Report, ATLAS TDR 1, CERN/LHCC 96-40 (1996).
- [2] ATLAS Collaboration, Liquid Argon Calorimeter Technical Design Report, ATLAS TDR 2, CERN/LHCC 96-41 (1996).
- [3] ATLAS Collaboration, Tile Calorimeter Technical Design Report, ATLAS TDR 3, CERN/LHCC 96-42 (1996).
- [4] ATLAS Collaboration (TILECAL), Z. Ajaltouni et al., CERN-PPE-96-178 (1996) 28 p., CERN, Geneva, Switzerland; Nucl. Instrum. Meth. A387 (1997) 333-351.
- [5] T.A. Gabriel and C. Zeitnitz, Nucl. Inst. Meth. A349 (1994) 106.
- [6] W.E. Cleland and E.G. Stern, Nucl. Inst. Meth. A338 (1994) 467.

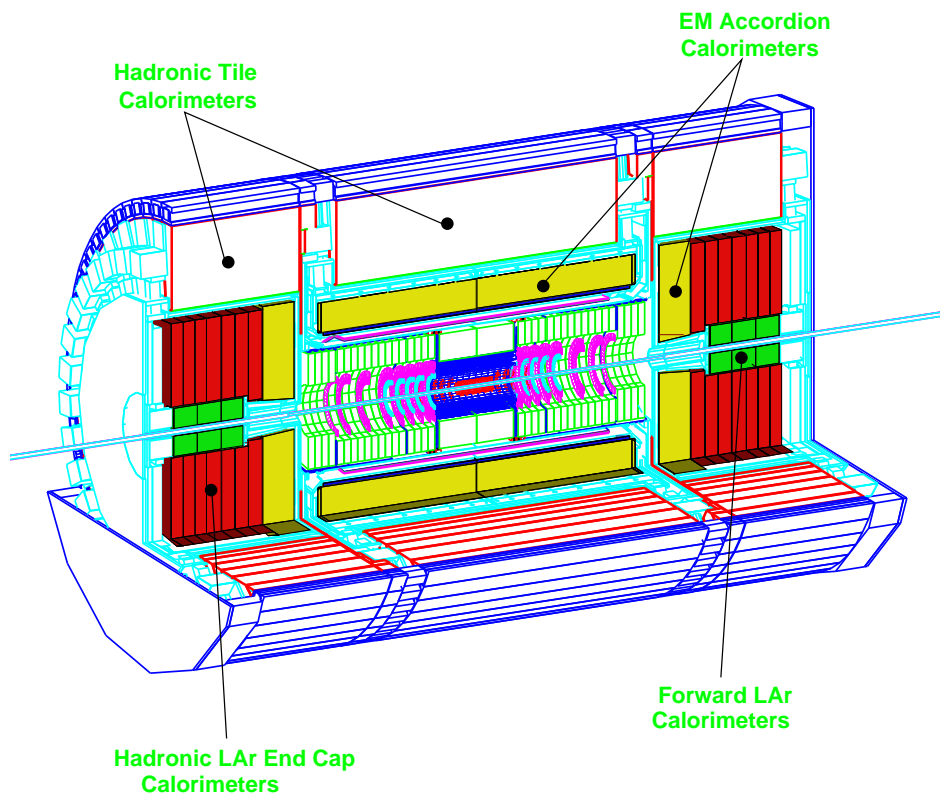


Figure 1: Three-dimensional cutaway view of the ATLAS calorimeters.

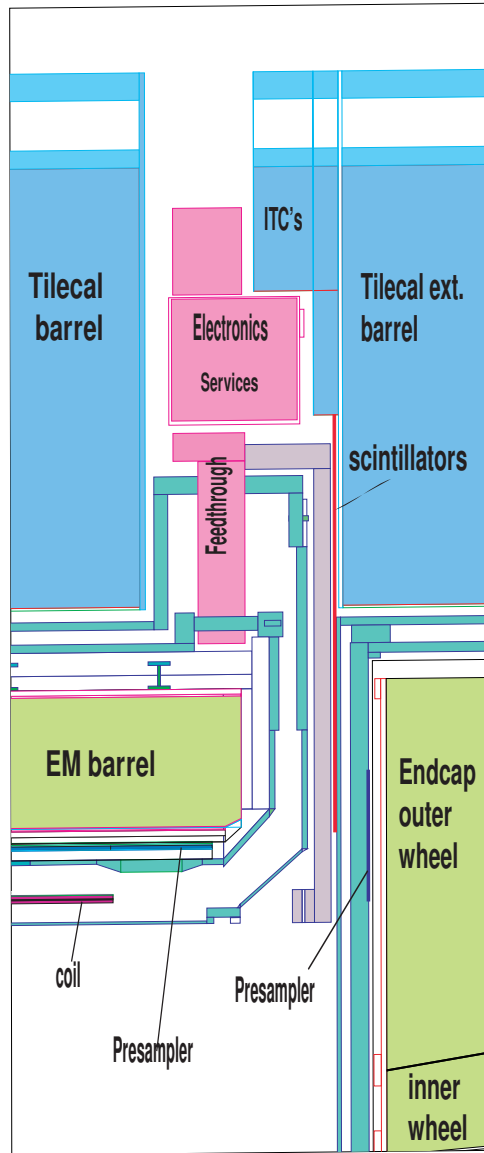


Figure 2: Longitudinal view of a quadrant of the vertical gap between the barrel and extended barrel Hadronic Tile Calorimeter.

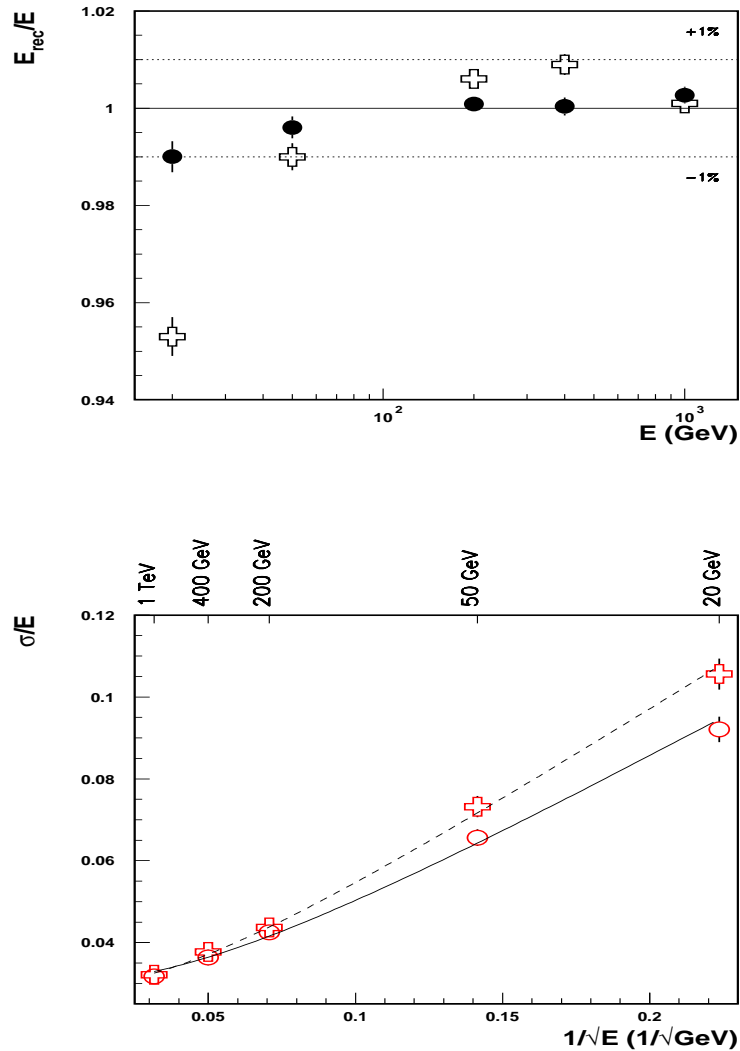


Figure 3: Pion energy scan in the central barrel ($\eta = 0.3$). The top plot shows the residual non-linearity, the bottom plot shows the energy resolution with the results of the fit with Equation $\sigma/E = a/\sqrt{E} \oplus b$. Two sets of parameters for the pion energy reconstruction have been used: open crosses — for energy independent parameters; solid dots — for parameters fitted at each energy and pseudorapidity.

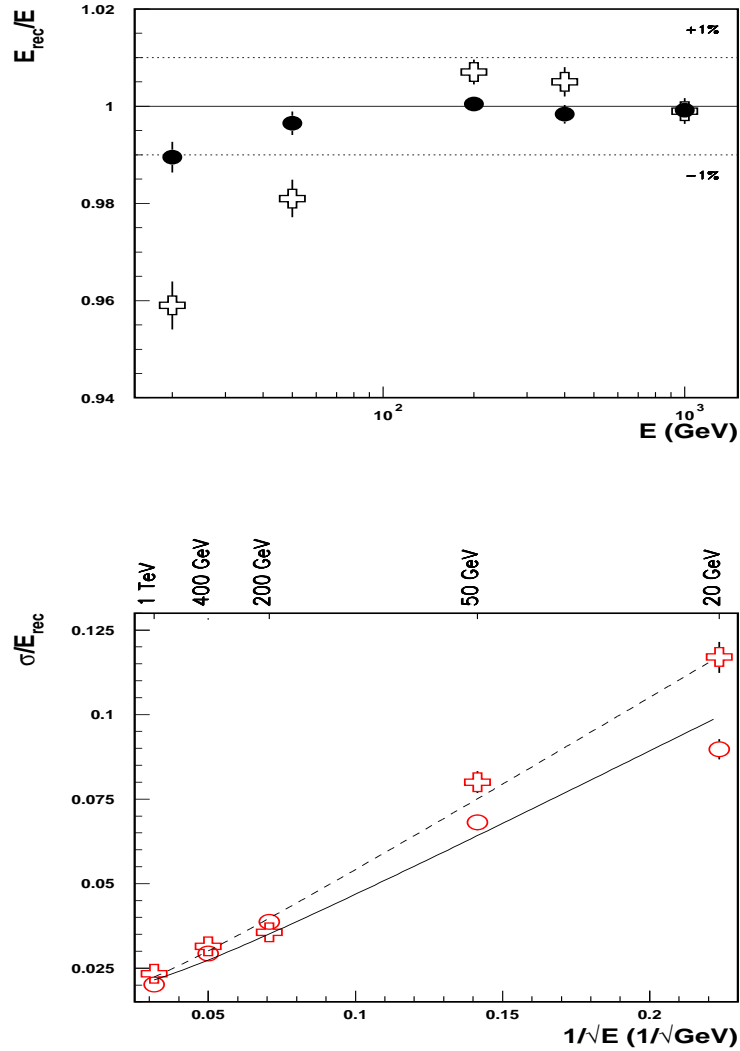


Figure 4: Pion energy scan in the extended barrel ($\eta = 1.3$). The top plot shows the residual non-linearity, the bottom plot shows the energy resolution with the results of the fit with Equation $\sigma/E = a/\sqrt{E} \oplus b$. Two sets of parameters for the pion energy reconstruction have been used: open crosses — for energy independent parameters; solid dots — for parameters fitted at each energy and pseudorapidity.

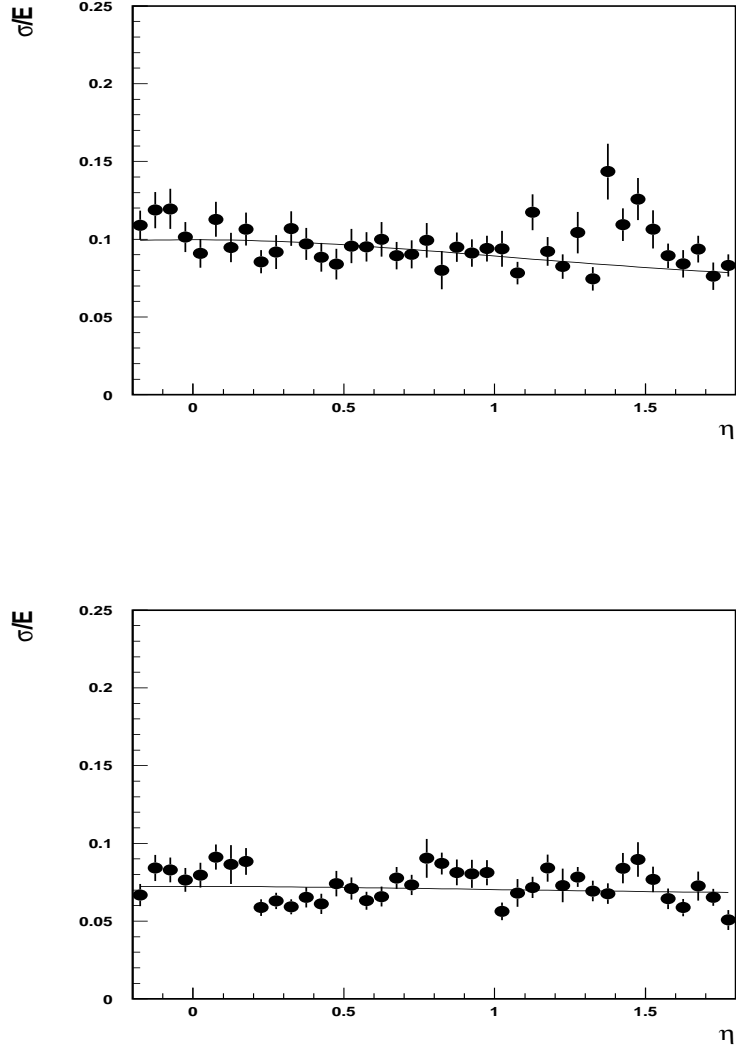


Figure 5: The dependence of the energy resolution on pseudorapidity for charged pions of constant transverse energy: $E_T = 20$ GeV (top plot) and $E_T = 50$ GeV (bottom plot). The lines correspond to the energy resolution parametrised using Equation $\sigma/E = 39\%/\sqrt{E} \oplus 1\%$ for $E_T = 20$ GeV and $\sigma/E = 49\%/\sqrt{E} \oplus 2\%$ for $E_T = 50$ GeV.

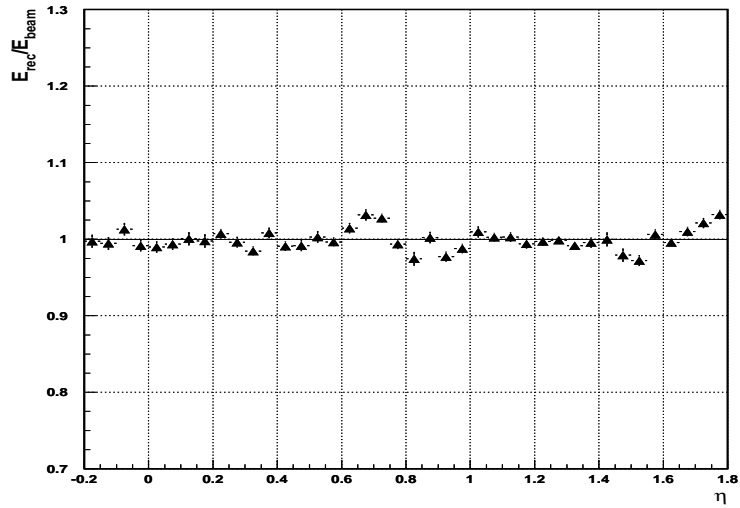
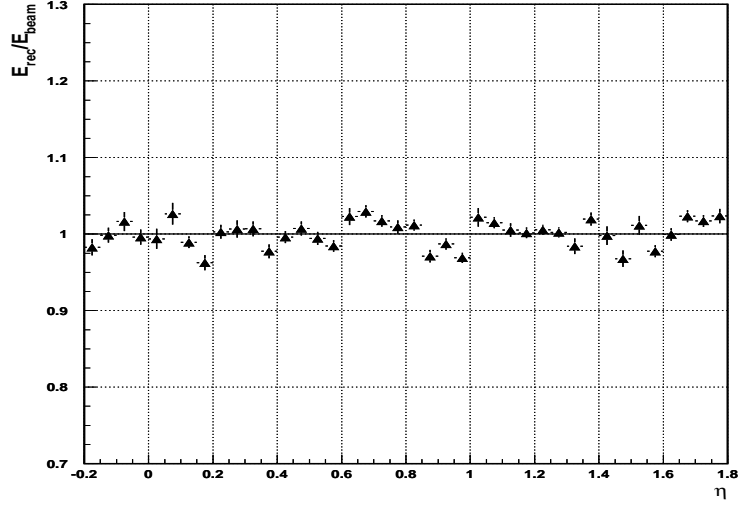


Figure 6: Single charged pion linearity across η : $E_T = 20$ GeV (top plot) and $E_T = 50$ GeV (bottom plot). Calibration coefficients are adjusted independently for each 0.4 bin in η but are kept constant within that interval. The figure shows the fitted mean of the pion distribution per bin of 0.05 in η .

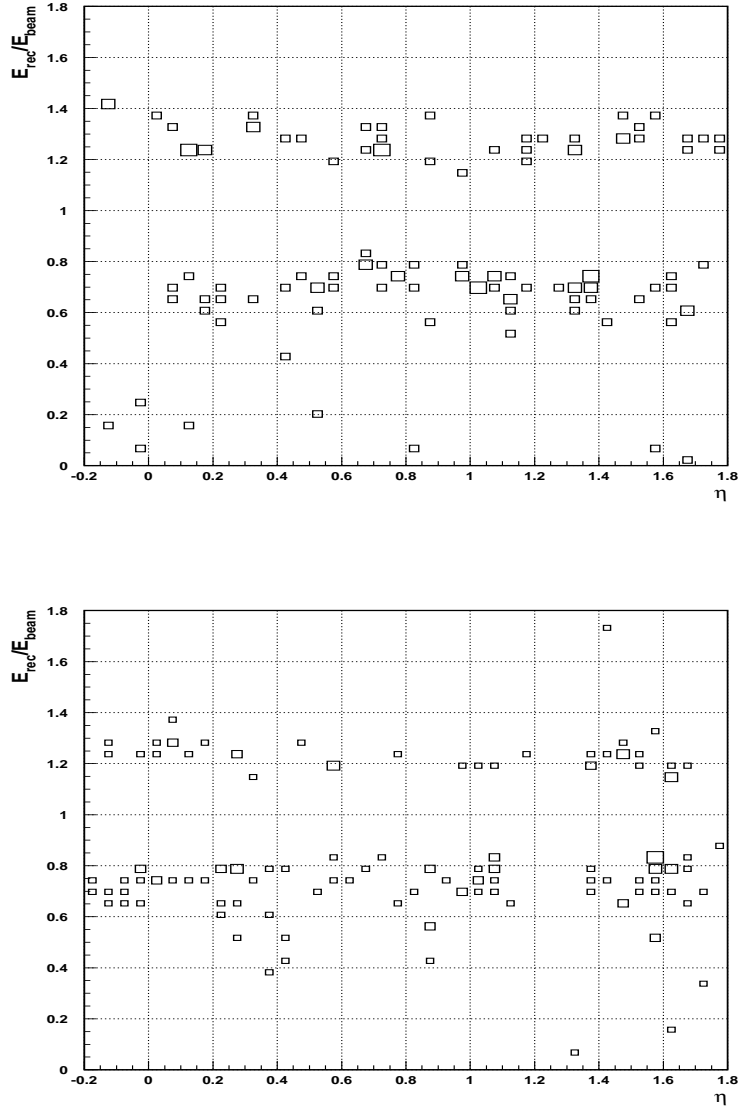


Figure 7: Events in the tails of the distribution of the reconstructed energy as a function of pseudorapidity for pions of $E_T = 20$ GeV (top plot) and $E_T = 50$ GeV (bottom plot). Tails are defined as events with reconstructed energies more than three standard deviations away from the mean.

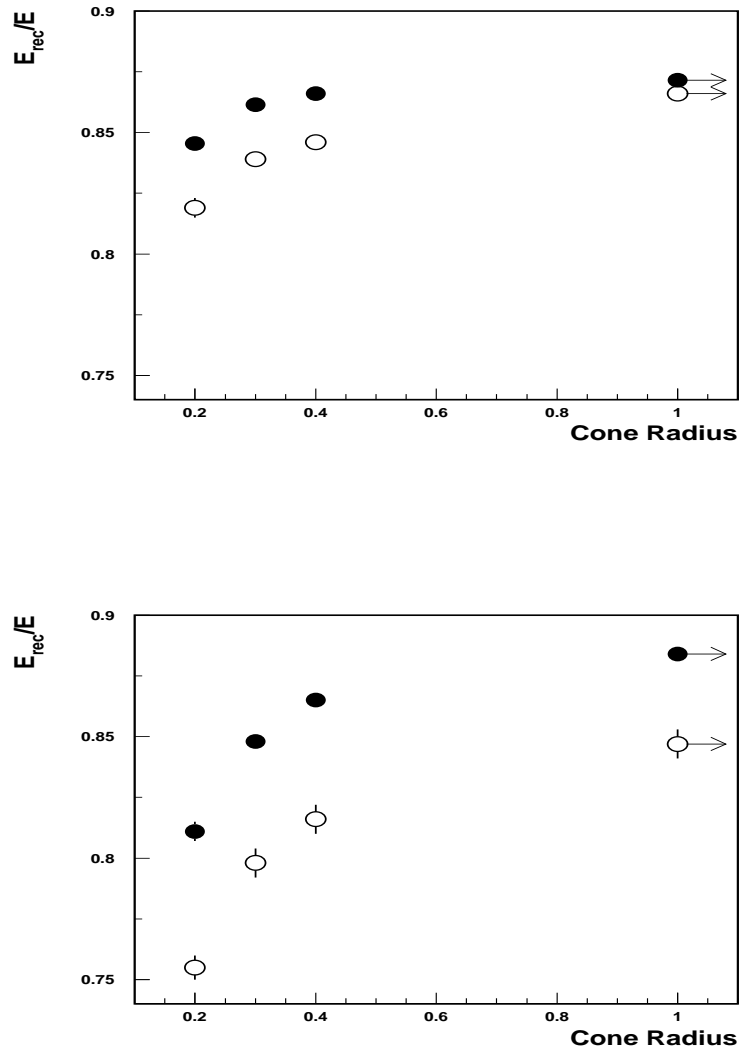


Figure 8: Energy response for 50 GeV (open circles) and 200 GeV (solid dots) charged pions at $\eta = 0.3$ (top plot) and $\eta = 1.3$ (bottom plot) as a function of the cone size. The points with arrows correspond to the case without restriction to a cone. Energy and pseudorapidity independent parameters were used for the energy reconstruction.

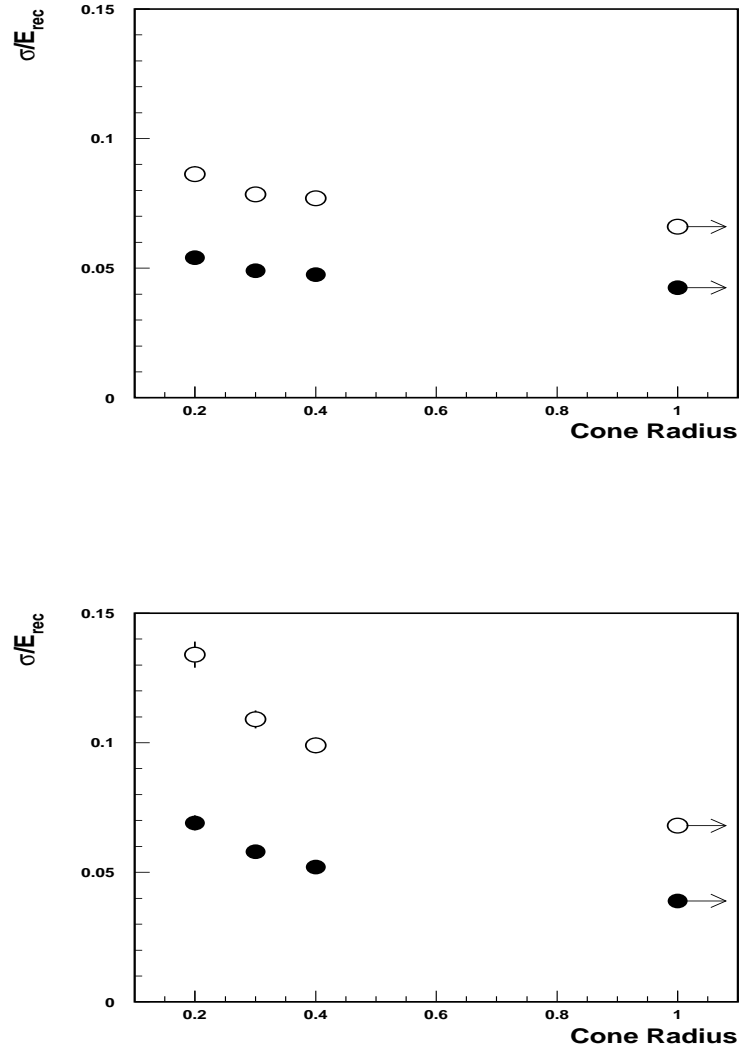


Figure 9: Energy resolution for 50 GeV (open circles) and 200 GeV (solid dots) charged pions at $\eta = 0.3$ (top plot) and $\eta = 1.3$ (bottom plot) as a function of the cone size. The points with the arrows correspond to the case without restriction to a cone. Energy and pseudorapidity dependent parameters were used for the energy reconstruction.

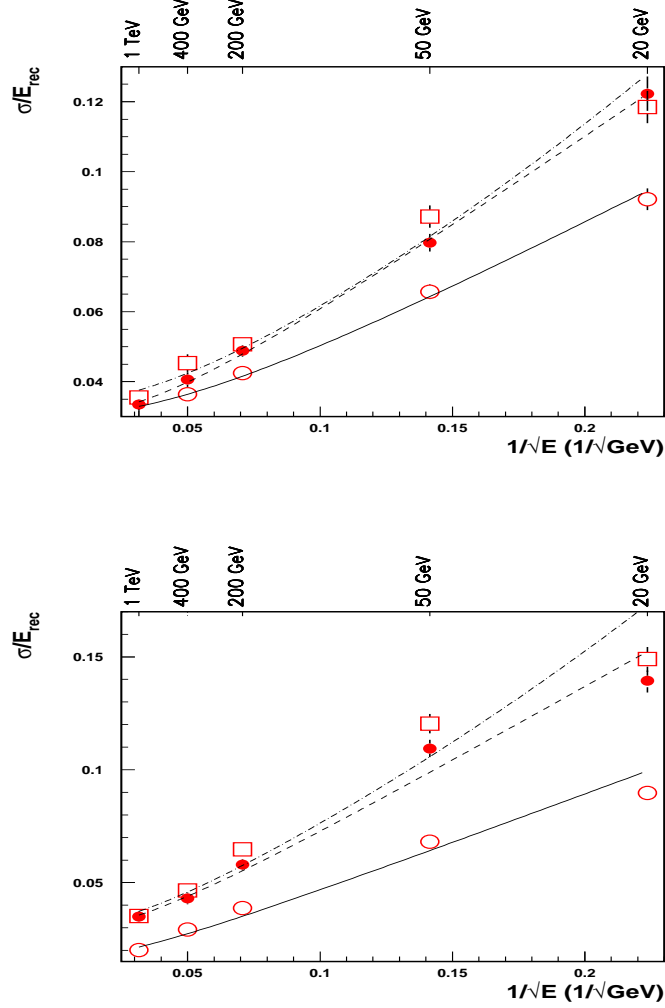


Figure 10: Energy dependence of the resolution for pions at $\eta = 0.3$ (top plot) and $\eta = 1.3$ (bottom plot). The open circles show the intrinsic calorimeter resolution obtained with no cut cone restriction and without electronic noise. The solid dots show results obtained for a cone of $\Delta R = 0.3$ and without electronic noise. The open squares show the results obtained for a cone of $\Delta R = 0.3$ and with a 2σ -noise cut (white electronic noise included). The curves show the results of the fits done with the two-term formula (3) for the first two sets and with the tree-term formula (4) for the third set.